24th INTERNATIONAL CONGRESS ON SOUND AND VIBRATION
23–27 July 2017, London

ACOUSTIC STREAMING IN RESONATORS WITH HEATED WALLS

Milan Červenka and Michal Bednařík
Czech Technical University in Prague, Faculty of Electrical Engineering Technická 2, 166 27 Prague 6, Czech Republic
email: milan.cervenka@fel.cvut.cz

Acoustic streaming in fluid-filled resonators with the spatial distribution of walls' temperature is studied within this work. The method of successive approximations is employed to derive linear equations for the calculation of ambient, primary acoustic, and time-averaged secondary fields including the mass transport velocity. The model equations have a standard form which allows their numerical integration using COMSOL Multiphysics. The numerical results are validated for the case of a resonator with spatially-constant ambient temperature by comparison with previously published analytical results; an excellent agreement is found. Examples of acoustic streaming structures in resonators with heated walls are given showing a strong influence on the walls' temperature distribution and the resonator cavity dimensions.

Keywords: acoustic streaming, resonator, finite element method

1. Introduction

Acoustic streaming [1, 2, 3] refers to a second-order net mean fluid flow generated by and superimposed on the first-order acoustic field. Within this work, an attention is paid to the boundary-layer-driven acoustic streaming generated in the standing wave of an acoustic resonator. This type of acoustic streaming plays an important role in thermoacoustics, see e.g. [4], or in acoustofluidics, see e.g. [5, 6]. Here, we are particularly focussed on the behaviour of acoustic streaming in the temperature-inhomogeneous fluids. This area is interesting from the practical point of view, as in thermoacoustics, acoustic streaming serves as a means of unwanted heat transport, reducing the efficiency of thermoacoustic devices; on the other hand, this effect could be employed for the cooling of hot objects [7]. From the theoretical point of view, the interaction with the thermal fields could be the cause of the discrepancies between theoretical predictions and the experimental data [8, 9].

Behaviour of acoustic streaming in temperature-inhomogeneous fluids can be, and has been studied in a rather straightforward way by the methods of the computational fluid dynamics [10, 11, 12, 13, 14, 15]. However, these methods require great amount of computational effort, which makes the study of acoustic streaming, especially in larger geometries, very difficult.

Within Section 2 of this paper, we propose a simplified mathematical model based on the method of successive approximations, allowing study of the interaction of acoustic streaming with a thermal fields using a reasonable computational resources. The numerical procedure, employing commercial software COMSOL Multiphysics, is briefly described in Section 3. Examples of numerical results are given in Section 4, some conclusions are drawn in Section 5.

2. Mathematical model

Theoretical study of acoustic streaming usually starts with Nevier-Stokes equations

$$\frac{\mathrm{d}\rho}{\mathrm{d}t} = -\rho\boldsymbol{\nabla}\cdot\boldsymbol{u}, \tag{1a}$$

$$\rho\frac{\mathrm{d}\boldsymbol{u}}{\mathrm{d}t} = \boldsymbol{\nabla}\cdot\boldsymbol{\sigma}+\boldsymbol{f}, \tag{1b}$$

$$\rho c_\mathrm{p}\frac{\mathrm{d}T}{\mathrm{d}t}-\alpha T\frac{\mathrm{d}p}{\mathrm{d}t} = \boldsymbol{\nabla}\cdot(\kappa\boldsymbol{\nabla}T)+\boldsymbol{\tau}:\boldsymbol{\nabla}\boldsymbol{u}, \tag{1c}$$

see e.g. [16], where ρ is the density, $\boldsymbol{u}$ is the velocity vector, T is the temperature, p is the pressure, $\boldsymbol{f}$ is the body force density, if the resonant channel is driven by an inertial force (by entire-body shaking) it reads $\boldsymbol{f}=-\rho\boldsymbol{a}(t)$, where $\boldsymbol{a}(t)$ is the channel's acceleration. Further, c_p is the specific heat capacity at constant pressure, α is the isobaric coefficient of volumetric thermal expansion and κ is the coefficient of thermal conduction. The total stress tensor $\boldsymbol{\sigma}$ is defined as

$$\boldsymbol{\sigma}=-p\boldsymbol{I}+\boldsymbol{\tau}=-p\boldsymbol{I}+\mu\left[\boldsymbol{\nabla}\boldsymbol{u}+(\boldsymbol{\nabla}\boldsymbol{u})^\mathrm{T}\right]-\frac{2\mu}{3}(\boldsymbol{\nabla}\cdot\boldsymbol{u})\boldsymbol{I}, \tag{2}$$

where $\boldsymbol{\tau}$ is the viscous stress tensor, μ is the shear viscosity, and $\boldsymbol{I}$ is the identity matrix. In this study, it is assumed that the shear viscosity and the coefficient of thermal conduction are temperature-dependent.

In Eqs. (1), the material derivative is defined as $\mathrm{d}(-)/\mathrm{d}t=\partial(-)/\partial+(\boldsymbol{u}\cdot\boldsymbol{\nabla})(-)$. It is assumed that the fluid is an ideal gas for which the state equation has the form $p=\rho RT$, where R is the specific gas constant and thus $\alpha=-(\partial\rho/\partial T)_p/\rho=1/T$.

Within this work, set of Eqs. (1) is solved using the method of successive approximations the same way as in work [17]. It is assumed that the field variables can be expressed as series

$$\begin{aligned} p&=p_0+\epsilon p_1+\epsilon^2p_2+\ldots, & \boldsymbol{u}&=\epsilon\boldsymbol{u}_1+\epsilon^2\boldsymbol{u}_2+\ldots,\\ \rho&=\rho_0+\epsilon\rho_1+\epsilon^2\rho_2+\ldots, & \boldsymbol{a}&=\epsilon\boldsymbol{a}_1,\\ T&=T_0+\epsilon T_1+\epsilon^2T_2+\ldots, \end{aligned}$$

where $\epsilon\ll 1$ is a small dimensionless parameter (corresponding to the acoustic Mach number), p_0, ρ_0 and T_0 are the ambient quantities (without sound) considered as constants in time. It is assumed that $p_0=const.$, $T_0=T_0(\boldsymbol{r})$ and $\rho_0=\rho_0(\boldsymbol{r})=p_0/RT_0(\boldsymbol{r})$. Further, p_1, ρ_1, T_1 and $\boldsymbol{u}_1$ are the primary acoustic variables supposed to be harmonic with angular frequency ω, which is the frequency of driving. The quantities with indices bigger than one are the nonlinearly generated terms; in this case, the terms with indices bigger than two are neglected.

Within the method of successive approximations, the above series are substituted into Eqs. (1) and the equations for the same order of ϵ are found.

For ϵ^0, we obtain

$$\boldsymbol{\nabla}\cdot(\kappa_0\boldsymbol{\nabla}T_0)=0, \tag{3}$$

where $\kappa_0=\kappa(T_0)$.

For ϵ^1, we can write

$$\frac{\partial\rho_1}{\partial t}+\boldsymbol{\nabla}\cdot(\rho_0\boldsymbol{u}_1)=0, \tag{4a}$$

$$\rho_0\frac{\partial\boldsymbol{u}_1}{\partial t}-\boldsymbol{\nabla}\cdot\left\{-p_1\boldsymbol{I}+\mu_0\left[\boldsymbol{\nabla}\boldsymbol{u}_1+(\boldsymbol{\nabla}\boldsymbol{u}_1)^\mathrm{T}\right]-\frac{2\mu_0}{3}(\boldsymbol{\nabla}\cdot\boldsymbol{u}_1)\boldsymbol{I}\right\}=-\rho_0\boldsymbol{a}_1, \tag{4b}$$

$$\rho_0c_{\mathrm{p}0}\left(\frac{\partial T_1}{\partial t}+\boldsymbol{u}_1\cdot\boldsymbol{\nabla}T_0\right)-\frac{\partial p_1}{\partial t}-\boldsymbol{\nabla}\cdot(\kappa_0\boldsymbol{\nabla}T_1)=0, \tag{4c}$$

where $c_{\mathrm{p}0} = c_{\mathrm{p}}(T_0)$, $\mu_0 = \mu(T_0)$, together with the linearised state equation $p_1/p_0 = T_1/T_0 + \rho_1/\rho_0$. Equations (4) can be used for calculation of the primary acoustic field.

For ϵ^2 the equations for the steady state, see e.g. [17], can be written in form

$$\boldsymbol{\nabla}\cdot(\rho_0\bar{\boldsymbol{u}}_2) = M, \tag{5a}$$

$$-\boldsymbol{\nabla}\cdot\left\{-\bar{p}_2\boldsymbol{I}+\mu_0\left[\boldsymbol{\nabla}\bar{\boldsymbol{u}}_2+(\boldsymbol{\nabla}\bar{\boldsymbol{u}}_2)^{\mathrm{T}}\right]-\frac{2\mu_0}{3}(\boldsymbol{\nabla}\cdot\bar{\boldsymbol{u}}_2)\boldsymbol{I}\right\} = \boldsymbol{F}, \tag{5b}$$

$$\rho_0 c_{\mathrm{p}0}\bar{\boldsymbol{u}}_2\cdot\boldsymbol{\nabla}T_0-\boldsymbol{\nabla}\cdot(\kappa_0\boldsymbol{\nabla}\bar{T}_2) = Q, \tag{5c}$$

where the bar denotes the one-period-averaged quantities.

The source terms in Eqs. (5) read

$$M = -\boldsymbol{\nabla}\cdot\langle\rho_1\boldsymbol{u}_1\rangle, \tag{6a}$$

$$\boldsymbol{F} = -\left\langle\rho_1\left(\boldsymbol{a}_1+\frac{\partial\boldsymbol{u}_1}{\partial t}\right)\right\rangle-\rho_0\langle(\boldsymbol{u}_1\cdot\boldsymbol{\nabla})\boldsymbol{u}_1\rangle + \boldsymbol{\nabla}\cdot\left\langle\frac{\mu_0 b_\mu}{T_0}T_1\left[\boldsymbol{\nabla}\boldsymbol{u}_1+(\boldsymbol{\nabla}\boldsymbol{u}_1)^{\mathrm{T}}-\frac{2}{3}(\boldsymbol{\nabla}\cdot\boldsymbol{u}_1)\boldsymbol{I}\right]\right\rangle, \tag{6b}$$

$$Q = -c_{\mathrm{p}0}\left\langle\rho_1\frac{\partial T_1}{\partial t}\right\rangle-\rho_0 c_{\mathrm{p}0}\langle\boldsymbol{u}_1\cdot\boldsymbol{\nabla}T_1\rangle-c_{\mathrm{p}0}\langle\rho_1\boldsymbol{u}_1\rangle\cdot\boldsymbol{\nabla}T_0+\langle\boldsymbol{u}_1\cdot\boldsymbol{\nabla}p_1\rangle + \boldsymbol{\nabla}\cdot\left\langle\frac{\kappa_0 b_\kappa}{T_0}T_1\boldsymbol{\nabla}T_1\right\rangle+\mu_0\left\langle\left[\boldsymbol{\nabla}\boldsymbol{u}_1+(\boldsymbol{\nabla}\boldsymbol{u}_1)^{\mathrm{T}}-\left(\frac{2}{3}-\tilde{V}\right)(\boldsymbol{\nabla}\cdot\boldsymbol{u}_1)\boldsymbol{I}\right]:\boldsymbol{\nabla}\boldsymbol{u}_1\right\rangle. \tag{6c}$$

where $\langle fg\rangle = \Re[\tilde{f}\tilde{g}^*]/2$; the tildes represent the complex amplitudes of the corresponding quantities and the asterisk stands for the complex conjugate. Further, $b_\mu = T_0(\partial\mu/\partial T)_{T_0}/\mu_0$ and $b_\kappa = T_0(\partial\kappa/\partial T)_{T_0}/\kappa_0$.

3. Numerical procedure

The formerly presented equations were solved numerically in axi-symmetric cylindrical coordinates using software COMSOL Multiphysics as follows.

First, ambient fluid temperature T_0 is calculated using the Heat Transfer in Fluids, Stationary study type, which implements Eq. (3). As a boundary condition, prescribed wall temperature distribution is used.

Second, primary-field quantities p_1, $\boldsymbol{u}_1$, T_1 and ρ_1 are calculated using the Linearised Navier-Stokes, Frequency-domain study type, which implements Eqs. (4). As the boundary conditions, isothermal no-slip ones were used at the walls; symmetry was employed at the symmetry-axis, see Fig. 1.

Third, time-averaged quantities $\bar{p}_2$, $\bar{\boldsymbol{u}}_2$, $\bar{T}_2$ and $\bar{\rho}_2$ are calculated using the Linearised Navier-Stokes, Frequency-domain study type (with frequency set to 0 Hz), which implements Eqs. (5). As the boundary conditions, isothermal no-slip ones were used at the walls; symmetry was employed at the symmetry-axis. The source terms (6) were evaluated using the primary-field quantities calculated in the previous step.

The numerical calculations were performed on a structured (mapped) mesh refined along the resonator walls.

4. Results

In all the numerical results presented below, air at normal atmospheric pressure was used as the medium filling the cylindrical resonator of length $L = 30$ cm and radius $R = 1.5$ cm.

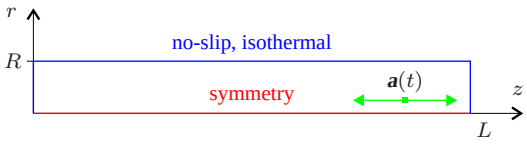

Figure 1: Geometry of the problem.

4.1 Comparison with an analytical model

In order to validate the numerical results, they were compared with the ones obtained using the analytical model [18] for the constant ambient fluid temperature, which was set to $T_0 = 20\,^{\circ}\mathrm{C}$. Driving acceleration with amplitude $a_1 = 5.49\,\mathrm{m/s^2}$ and direction along the channel axis was used for driving; the frequency of driving was set to the first resonance frequency $f_{\mathrm{res}} = 569.2\,\mathrm{Hz}$. In this case, the ratio of the resonator radius and the viscous boundary layer thickness $R/\delta_{\mathrm{v}} = 163.4$, where $\delta_{\mathrm{v}} = \sqrt{2\mu/\rho_0\omega}$.

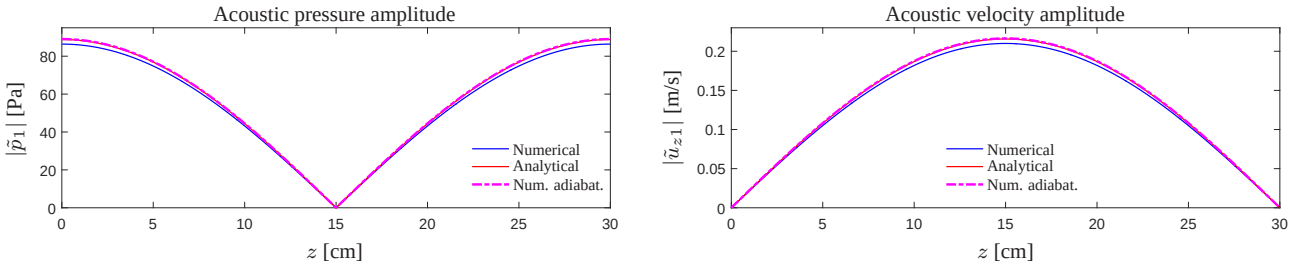

Figure 2: Acoustic pressure and velocity amplitude distribution along the axis of a resonator driven at the $\lambda/2$ resonance.

Figure 2 shows the comparison of the primary-field quantities along the resonator axis. It can be seen that the numerical model (blue line) predicts lower amplitudes than the analytical model (red line). This is caused by the fact that the analytical model [18] does not take into account thermal losses at the resonator end-walls ($z = 0$ and $z = L$). If these losses are removed from the numerical model (by imposing the adiabatic end-walls), the analytical model and the numerical model (pink line) provides the same results.

The streaming velocity (z-component) calculated using the current model is compared with the Rott's approximate formula [19, 18] valid for $R \gg \delta_{\mathrm{v}}$:

$$\bar{u}_z = u_{\mathrm{R}} \left[1 + \frac{2}{3}(\gamma - 1)(1 - b_\mu) \frac{\sqrt{\mathrm{Pr}}}{1 + \mathrm{Pr}} \right] \left(1 - \frac{2r^2}{R^2} \right) \sin 2kz, \qquad u_{\mathrm{R}} = \frac{3}{8} \frac{u_0^2}{c_0}, \tag{7}$$

where γ is the adiabatic exponent, Pr is the Prandtl number, k is the wavenumber, c_0 is the speed of sound, and u_0 is the maximum longitudinal velocity amplitude along the resonator axis. The quantity u_{R} is so-called Rayleigh streaming velocity.

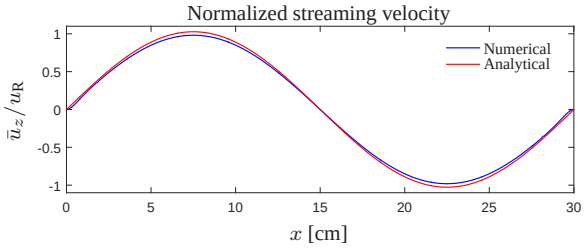

Figure 3: Normalized streaming velocity along the resonator axis; driving at the $\lambda/2$ resonance.

Figure 3 shows the streaming velocity along the resonator axis normalized by the Rayleigh velocity calculated by the current model (blue line) and employing the Rott's formula (7) (red line). It can be seen that the numerical and analytical results slightly differ, which can be attributed to the simplifications in Eq. (7).

4.2 Streaming in temperature-inhomogeneous fluid

Let's assume the resonator walls with the temperature distribution given as

$$T_{\mathrm{w}} = \frac{\Delta T}{2}\left[1 + \cos\left(\frac{2\pi z}{L}\right)\right] + T_{\mathrm{w0}}, \tag{8}$$

where T_{w0} is the minimum temperature of the resonator walls and ΔT is the maximum temperature difference. The formula (8) serves as the boundary condition for Eq. (3) for calculation of the fluid ambient temperature $T_0(\boldsymbol{r})$. In all the following cases, $T_{\mathrm{w0}} = 20\,^{\circ}\mathrm{C}$ and temperatures ΔT differ.

The wall temperature distribution (8) corresponds to the case of the thermoacoustically-driven heat transport along the resonator walls from acoustic-velocity antinode towards the acoustic-velocity nodes, see e.g.[8].

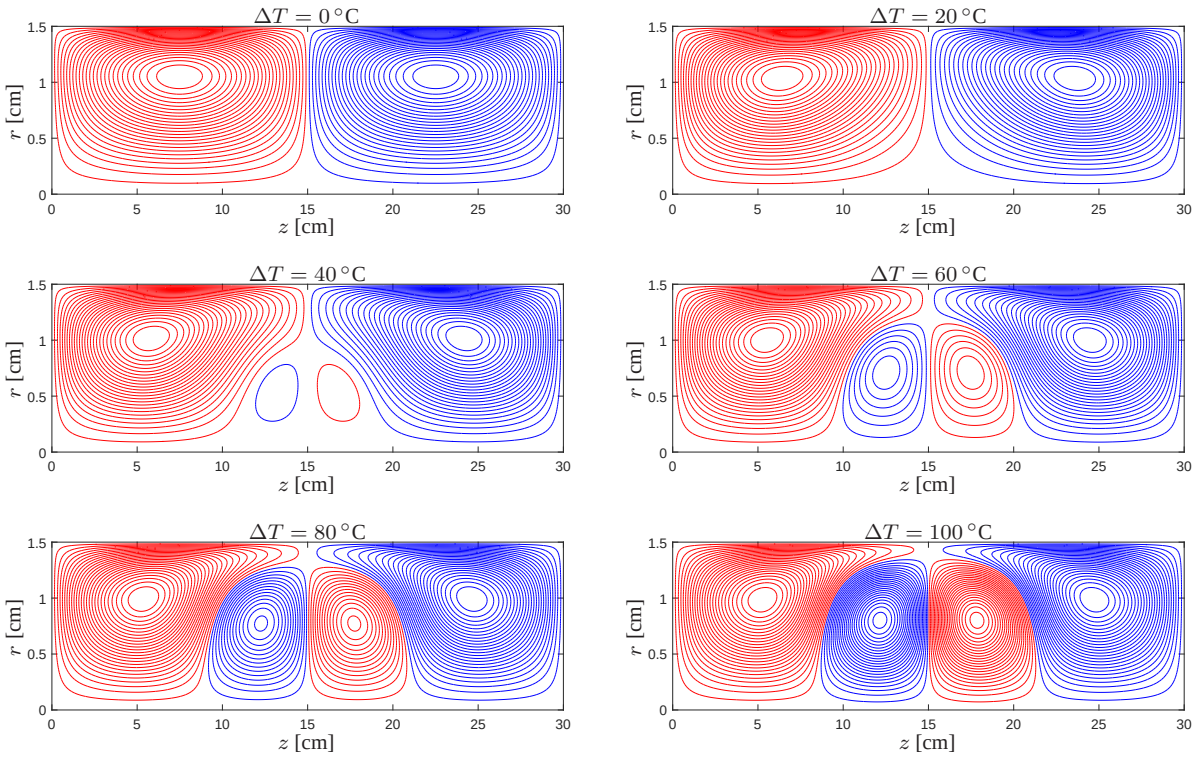

Figure 4: Streaming in the resonator with individual temperature differences $\Delta T = 0, 20, 40, 60, 80, 100\,^{\circ}\mathrm{C}$; driving at $\lambda/2$ resonance frequency.

Figure 4 shows the streamlines in the resonator for individual values of $\Delta T = 0, 20, 40, 60, 80$, and $100\,^{\circ}\mathrm{C}$. In all the cases, the resonator is driven at its first resonance frequency. The counter-clockwise-rotating streaming cells are depicted in red colour, the clockwise-rotating streaming cells are depicted in blue colour. It can be observed that with increasing temperature difference ΔT, additional outer vortices appear in the centre of the resonator.

The reason for emergence of the additional streaming cells can be seen in Fig. 5. The imposed temperature inhomogeneity supports the streaming near the resonator ends (streaming velocity increases); whereas the streaming is opposed in the central part – streaming velocity decreases and for $\Delta T \gtrapprox 30\,^{\circ}\mathrm{C}$. the streaming velocity reverses its direction giving rise to the emergence of the additional vortices.

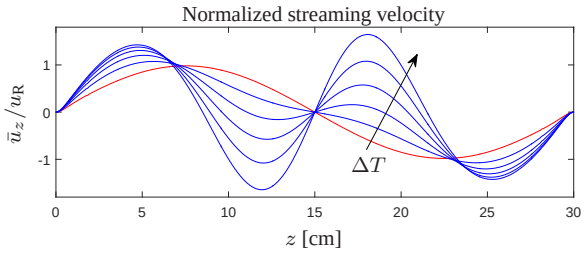

Figure 5: Normalized streaming velocity along the resonator axis for individual values of the temperature difference $\Delta T = 0, 20, 40, 60, 80, 100\,^{\circ}\mathrm{C}$.

5. Conclusions

Linearised model equations have been derived for the description of the primary as well as steady-state secondary fields in acoustic resonators with heated walls. These equations have a standard form of linearised Navier-Stokes equations, so that they can be solved in a straightforward way employing an universal solver; in this case, COMSOL Multiphysics was used.

The numerical results show that the fluid temperature inhomogeneity can result in the appearance of additional vortices, if the temperature difference is big enough. The additional vortices appear (are more prominent) for bigger rations R/δ_{v}.

The proposed mathematical model takes into account the influence of temperature inhomogeneity on the acoustic and steady-state streaming field, however, it does not account for the acoustic streaming as a means of the advective heat transport, which influences back the fluid temperature distribution. It means that the proposed model is only valid for small values of the streaming velocity. Addressing this issue would require a more comprehensive mathematical model, which is the subject of our future work. In any case, the current results indicate that the streaming dynamics in temperature-inhomogeneous fields, thanks to the feedback effects, can be rather complex.

Acknowledgements

This work was supported by GACR grant No. 15-23079S and by The Ministry of Education, Youth and Sports from the Large Infrastructures for Research, Experimental Development and Innovations project “IT4Innovations National Supercomputing Center – LM2015070.”

REFERENCES

1. Rudenko, O. V. and Soluyan, S. I., *Theoretical Foundations of Nonlinear Acoustics*, Consultants Bureau, New York (1977).

2. Nyborg, W. L., (1998), Acoustic streaming. Hamilton, M. F. and Blackstock, D. T. (Eds.), *Nonlinear Acoustics*, pp. 207–231, Academic Press.

3. Boluriaan, S. and Morris, P. J. Acoustic streaming: from Rayleigh to today, *Int. J. Aeroacoust.*, **2** (3+4), 255–292, (2003).

4. Swift, G. W., *Thermoacoustics: A unifying perspective for some engines and refrigerators*, Acoustical Society of America, Melville, New York (2002).

5. Green, R., Ohlin, M. and Wiklund, M., (2015), Applications of acoustic streaming. Laurell, T. and Lenshof, A. (Eds.), *Microscale Acoustofluidics*, pp. 312–336, The Royal Society of Chemistry.

6. Muller, P. B., Barnkob, R., Jensen, M. J. H. and Bruus, H. A numerical study of microparticle acoustophoresis driven by acoustic radiation forces and streaming-induced drag forces, *Lab on a Chip*, **12**, 4617–4627, (2012).

7. Mozurkewich, G. Heat transport by acoustic streaming within a cylindrical resonator, *Appl. Acoust.*, **63**, 713–735, (2002).

8. Thompson, M. W., Atchley, A. A. and Maccarone, M. J. Influences of a temperature gradient and fluid inertia on acoustic streaming in a standing wave, *J. Acoust. Soc. Am.*, **117**, 1839–1849, (2005).

9. Reyt, I., Daru, V., Bailliet, H., Moreau, S., Valière, J.-C., Baltean-Carlès, D. and Weisman, C. Fast acoustic streaming in standing waves: generation of an additional outer streaming cell, *J. Acoust. Soc. Am.*, **134**, 1791–1801, (2013).

10. Gubaidullin, A. A. and Yakovenko, A. V. Effects of heat exchange and nonlinearity on acoustic streaming in a vibrating cylindrical cavity, *J. Acoust. Soc. Am.*, **137**, 3281–3287, (2015).

11. Aktas, M. K. and Farouk, B. Numerical simulation of acoustic streaming generated by finite-amplitude resonant oscillations in an enclosure, *J. Acoust. Soc. Am.*, **116**, 2822–2831, (2004).

12. Daru, V., Baltean-Carlès, D., Weisman, C., Debesse, P. and Gandikota, G. Two-dimensional numerical simulations of nonlinear acoustic streaming in standing waves, *Wave Motion*, **50**, 955–963, (2013).

13. Aktas, M. K., Farouk, B. and Lin, Y. Heat transfer enhancement by acoustic streaming in an enclosure, *J. Heat Transf.*, **127**, 1313–1321, (2005).

14. Lin, Y. and Farouk, B. Heat transfer in a rectangular chamber with differentially heated horizontal walls: Effects of a vibrating sidewall, *Int. J. Heat Mass Tran.*, **51**, 3179–3189, (2008).

15. Aktas, M. K. and Ozgumus, T. The effects of acoustic streaming on thermal convection in an enclosure with differentially heated horizontal walls, *Int. J. Heat Mass Tran.*, **53**, 5289–5297, (2010).

16. Lautrup, B., *Physics of Continuous Matter, Second Edition: Exotic and Everyday Phenomena in the Macroscopic World*, CRC Pres, Boca Raton (2011).

17. Červenka, M. and Bednařík, M. Variety of acoustic streaming in 2D resonant channels, *Wave Motion*, **66**, 21–30, (2016).

18. Hamilton, M. F., Ilinskii, Y. A. and Zabolotskaya, E. A. Thermal effects on acoustic streaming in standing waves, *J. Acoust. Soc. Am.*, **114**, 3092–3101, (2003).

19. Rott, N. The influence of heat conduction on acoustic streaming, *Z. Angew. Math. Phys.*, **25**, 417–421, (1974).